Higgs Mode in the d-Wave Superconductor Bi_{2}Sr_{2}CaCu_{2}O_{8+x} Driven by an Intense Terahertz Pulse

Kota Katsumi, Naoto Tsuji, Yuki I. Hamada, Ryusuke Matsunaga, John Schneeloch, Ruidan D. Zhong, Genda D. Gu, Hideo Aoki, Yann Gallais, and Ryo Shimano

Phys. Rev. Lett. **120**, 117001 — Published 14 March 2018

DOI: 10.1103/PhysRevLett.120.117001

Higgs mode in the *d*-wave superconductor $Bi_2Sr_2CaCu_2O_{8+x}$ driven by an intense terahertz pulse

Kota Katsumi[1], Naoto Tsuji[2], Yuki I. Hamada[1], Ryusuke Matsunaga[1,3], John Schneeloch[4], Ruidan D. Zhong[4], Genda. D. Gu[4], Hideo Aoki[1,5,6], Yann Gallais[1,7,8] and Ryo Shimano[1,8]

[1] Department of Physics, The University of Tokyo, Tokyo, 113-0033, Japan

[2] RIKEN Center for Emergent Matter Science (CEMS), Wako, 351-0198, Japan

[3]JST, PRESTO, Kawaguchi, 332-0012, Japan

[4] Brookhaven National Lab, Upton, NY, 11973, USA

[5] Department of Physics, ETH Zürich, 8093 Zürich, Switzerland

[6] National Institute of Advanced Industrial Science and Technology (AIST), Tsukuba, 305-8568, Japan

[7] MPQ CNRS, Université Paris Diderot, Bâtiment Condorcet, 75205 Paris Cedex 13, France

[8] Cryogenic Research Center, The University of Tokyo, Tokyo, 113-0032, Japan

Abstract

We investigated the terahertz (THz)-pulse driven nonlinear response in the *d*-wave cuprate superconductor $Bi_2Sr_2CaCu_2O_{8+x}$ (Bi2212) using a THz pump near-infrared probe scheme in the time domain. We have observed an oscillatory behavior of the optical reflectivity that follows the THz electric field squared and is markedly enhanced below T_c. The corresponding third-order nonlinear effect exhibits both A_{1g} and B_{1g} symmetry components, which are decomposed from polarization-resolved measurements. Comparison with a BCS calculation of the nonlinear susceptibility indicates that the A_{1g} component is associated with the Higgs mode of the *d*-wave order parameter.

PACS numbers:

74.40.Gh, Nonequilibrium processes in superconductivity

74.25.Gz, Optical properties of superconductivity

78.47.J-, Pump-probe spectroscopy in ultrafast solid state dynamics

In a superconductor the spontaneous breaking of $U(1)$ phase leads to two types of collective excitations of the order parameter. One is the Nambu-Goldstone mode which is pushed up to the plasma frequency due to the Coulomb interaction, while the other is the amplitude (Higgs) mode [1,2]. Being chargeless and spinless, the Higgs mode in superconductors only weakly couples to external probes, and has thus remained elusive experimentally until recently even for conventional *s*-wave superconductors. The Higgs mode has been initially identified in a Raman measurement in $NbSe_2$, where the charge-density wave (CDW) coexists with superconductivity and makes the mode Raman-active via its indirect coupling to the CDW order parameter [3–5]. Recently, the Higgs mode has been clearly observed in a more generic situation (without CDW) in an *s*-wave superconductor $Nb_xTi_{1-x}N$ (NbN) by ultrafast terahertz (THz) pump-THz probe spectroscopy [6]. The role of the ultrashort THz-pump pulse is to provide a non-adiabatic quench of the order parameter by instantaneously creating a population of unpaired quasiparticles (QPs) around the superconducting (SC) gap energy that triggers Higgs oscillations in the time domain [7]. The Higgs dynamics of the SC order parameter has since been theoretically studied in a variety of contexts, extending to multiband or unconventional superconductors [8–12]. Specifically, in a *d*-wave superconductor such as the high-T_c cuprates with nodes in the gap function, the Higgs mode was theoretically shown to decay much faster than in the *s*-wave case because of the presence of low-energy QPs [9]. Besides, in many unconventional superconductors the coexistence with other electronic orders and/or competing interactions can significantly alter the Higgs-mode dynamics, and may lead to a rich assortment of collective modes [8,13–16]. Thus it is imperative to explore how the Higgs mode behaves in unconventional superconductors.

In this context, nonlinear optical effects have recently kicked off an alternative way to probe the Higgs mode [17,18]. This was demonstrated in the conventional *s*-wave superconductor NbN, where, remarkably, a resonance between the Higgs mode and an intense THz field with a photon energy ω below the SC gap 2Δ was shown to induce large third-harmonic generation (THG) with a resonance condition $2\omega = 2\Delta$ [17,18]. It has subsequently been pointed out that, in addition to the Higgs mode, charge density fluctuations (CDF) can also contribute to the THG signal at the same frequency [19]. Within the BCS mean-field approximation, the contribution of CDF to THG should be much larger

than the Higgs-mode contribution. More recently, the contributions from the Higgs mode and CDF have been decomposed in NbN via polarization-resolved measurements. The decomposition, theoretically shown to hold even beyond the BCS approximation, has revealed that the Higgs mode actually gives a dominant contribution to the THG far exceeding the CDF contribution [20]. Physically, the dominance of the Higgs mode in THG can be attributed to dynamical effects in the pairing, such as the retardation effects in the phonon-mediated electron interaction that are neglected in the BCS approximation [21]. Given this situation for the conventional *s*-wave superconductors, what happens in *d*-wave superconductors becomes of great interest.

In this Letter, we report an observation of the third-order nonlinear signal in a *d*-wave cuprate superconductor $Bi_2Sr_2CaCu_2O_{8+x}$ (Bi2212) from THz pump-optical reflectivity probe measurements over a wide range of carrier doping. The third-order nonlinear signal, akin to a THz Kerr effect, turns out to manifest itself as an oscillatory behavior of the optical reflectivity that follows the squared THz electric field (E-field) with strong enhancement below T_c. The THz Kerr signal is here further decomposed into A_{1g} and B_{1g} symmetry components from polarization-resolved measurements. We then show that a comparison with BCS calculations for both Higgs-mode and CDF contributions to each symmetry component strongly indicates that the observed A_{1g} component arises from the coupling of the *d*-wave order parameter to the Higgs mode.

We have performed a THz pump-optical probe (TPOP) measurements, schematically illustrated in Fig. 1(a), on freshly cleaved optimally-doped (OP90, $T_c \approx 90$ K) as well as overdoped (OD78, OD66 and OD52, with $T_c \approx 78$, 66, 52 K, respectively) and underdoped (UD74 and UD58, with $T_c \approx 74$, 58 K, respectively) Bi2212 single crystals grown with the floating-zone method. The description of the THz pulse generation is given in Supplemental Material (SM) [22]. For the probe we used a near-infrared pulse at 800 nm, which has been widely used as a sensitive probe for investigating the dynamics of the SC state in the cuprates [28–36]. The measurements were performed as a function of both the pump and probe polarization angles θ_{Pump}, θ_{Probe} as defined in Fig. 1(b). As we shall show, the polarization dependence of the pump-probe signal is crucial in discriminating the Higgs-mode and CDF contributions. The central frequency component of the THz-pump E-field is ~ 0.6 THz = 2.4 meV, which is much smaller than the anti-nodal SC gap energy,

$2\Delta_0 > 20$ meV, in Bi2212 for the present doping levels [37,38]. This THz pulse does not significantly deplete the SC state, as evidenced by the absence of any sign of pump-probe signal-saturation up to ~ 350 kV/cm (see SM Fig. S2).

Let us start with the result for optimally-doped OP90. The THz pulse-induced transient reflectivity change ΔR for $\theta_{\text{Pump}} = \theta_{\text{Probe}} = 0°$ is shown in Fig. 1(c) at various temperatures. At 30 K below T_c, an oscillatory behavior of $\Delta R/R$ that follows the squared THz-pump E-field $|E_{\text{Pump}}(t)|^2$ is clearly identified. This quasi-instantaneous oscillatory component, which we shall assign to the THz Kerr signal below, is similar to the forced oscillation of the order parameter observed in a conventional *s*-wave superconductor NbN, which also follows $|E_{\text{Pump}}(t)|^2$ [6]. Accordingly, the maximum amplitude of $\Delta R/R$ is proportional to the square of the peak THz-pump E-field as shown in SM Fig. S2. In addition to the THz Kerr component, $\Delta R/R$ has a positive decaying component that survives up to at least ~ 10 ps. At 100 K slightly above T_c, the signal consists of a much weaker THz Kerr component and a decaying signal that switches sign after ~ 4 ps. At 300 K the decaying signal remains positive at all delays.

The amplitude of $\Delta R/R$ as a function of θ_{Probe}, at a fixed delay $t = 2$ ps at which the THz Kerr component is maximum, is displayed in Fig. 1(d). The $\Delta R/R$ is essentially independent of the angle at 300 K and 100 K. At 30 K below T_c, however, it displays significant dependence on θ_{Probe}, which follows a form $A + B\cos(2\theta_{\text{Probe}})$. By contrast the $\Delta R/R$ signal at $t = 4$ ps does not show any polarization dependence at 30 K. Similar results were obtained when the pump polarization angle θ_{Pump} is varied with a fixed $\theta_{\text{Probe}} = 0°$, demonstrating symmetrical roles played by the pump and probe polarization angles in the observed signal (see SM Fig. S3(a)).

The pump E-field and polarization dependences of the oscillatory component are consistent with a THz Kerr effect, where the strong THz E-field modulates the optical reflectivity in the near-infrared (800 nm) regime [39]. This process is described by a third-order nonlinear susceptibility $\chi^{(3)}(\omega;\ \omega,\ +\Omega,\ -\Omega)$ [40], where ω and Ω are the frequencies of the near-infrared pulse and THz-pump pulse, respectively. The THz pulse-induced reflectivity change $\Delta R/R$ can be expressed in terms of $\chi^{(3)}$ (for details see SM) as

$$\frac{\Delta R}{R}(E_i^{\text{Probe}}, E_j^{\text{Probe}}) \sim \frac{1}{R}\frac{\partial R}{\partial \varepsilon_1}\, \varepsilon_0 \text{Re}\chi^{(3)}_{ijkl} E_k^{\text{Pump}} E_l^{\text{Pump}}, \quad (1)$$

where E_i denotes the ith component of the THz-pump or probe E-field and ε_1 is the real part of the dielectric constant. Assuming tetragonal symmetry for Bi2212, we can analyze the polarization dependence of $\chi^{(3)}(\theta_{\text{Pump}}, \theta_{\text{Probe}})$ in terms of the irreducible representations of D_{4h} point group as

$$\chi^{(3)}(\theta_{\text{Pump}},\theta_{\text{Probe}}) = \frac{1}{2}(\chi^{(3)}_{A_{1g}} + \chi^{(3)}_{B_{1g}} \cos 2\theta_{\text{Pump}} \cos 2\theta_{\text{Probe}} + \chi^{(3)}_{B_{2g}} \sin 2\theta_{\text{Pump}} \sin 2\theta_{\text{Probe}}), \quad (2)$$

where we have defined $\chi^{(3)}_{A_{1g}} = \chi^{(3)}_{xxxx} + \chi^{(3)}_{xxyy}$, $\chi^{(3)}_{B_{1g}} = \chi^{(3)}_{xxxx} - \chi^{(3)}_{xxyy}$ and $\chi^{(3)}_{B_{2g}} = \chi^{(3)}_{xyxy} + \chi^{(3)}_{xyyx}$.

For a given θ_{Pump}, the A_{1g} and B_{1g} signals respectively correspond to the isotropic and $\cos 2\theta_{\text{Probe}}$ components observed in Fig. 1(d), which can be extracted by adding or subtracting $\Delta R/R$ ($\theta_{\text{Probe}} = 0°$) and $\Delta R/R$ ($\theta_{\text{Probe}} = 90°$). As expected from Eq. (2) the extracted A_{1g} signal is found to be independent of θ_{Pump}, while the B_{1g} signal follows $\cos 2\theta_{\text{Pump}}$ (see Fig. S3(b)). On the other hand, no B_{2g} signal, obtained by subtracting $\Delta R/R$ ($\theta_{\text{Probe}} = 45°$) from $\Delta R/R$ ($\theta_{\text{Probe}} = -45°$), is observed within the noise level (10^{-5}) (see Fig. SM S4). We stress that the $B_{1/2g}$ THz Kerr signals discussed here are not linked to any symmetry breaking order, but simply follow from the general properties of susceptibility tensors for D_{4h} point group.

In Figs. 2(a) and 2(b) we present the temperature dependences of the A_{1g} and B_{1g} signals for OP90. For both symmetries the signal strongly evolves below T_c in the interval (1-2 ps), corresponding to the oscillatory component or THz Kerr signal discussed above. The decaying component at longer delays ($t > 4$ ps) is only observed in A_{1g} symmetry, and displays a more complex temperature dependence. To obtain more detailed information on the temperature dependence of the symmetry-resolved components, we fitted the transient signals with $|E_{\text{Pump}}(t)|^2$ (for the THz Kerr signal), an error function (decaying component) and a step function (offset component). In addition, $|E_{\text{Pump}}(t)|^2$ was convoluted with an exponential function to take account of a small delay (~ 200 fs) in the nonlinear response of the system [41] (see SM). The fitted result at 10 K is shown with the solid curves in Fig. 2(c).

Figure 2(d) summarizes the amplitudes of the different components of the A_{1g} and B_{1g} signals against temperature. The A_{1g} and B_{1g} THz Kerr components sharply increase below

T_c, indicating the onset of a new channel in the THz Kerr response upon entering the SC state. Contrary to the A_{1g} THz Kerr component which remains positive at all the temperatures, the decaying component switches sign twice, at T_c and T^*, respectively. Here T^* is within the range of the pseudogap (PG) temperature as determined by ARPES [42]. The decaying component also displays a sharp maximum slightly below T_c. The overall behavior of the decaying component, including the sign changes, is in good agreement with previous optical pump-optical probe (OPOP) measurements [32]. In these measurements the positive decaying component below T_c and the negative decaying component above T_c were assigned to QP relaxation in the SC and PG states, respectively.

Let us now turn to what happens when the doping level is varied. In all the samples, a THz Kerr component of $\Delta R/R$ was found to be strongly enhanced below T_c (with T-dependent temporal behavior shown in SM Fig. S6 for UD74 and OD78). The result for T = 10 K is shown in Figs. 3(a)-3(c) for UD74, OP90 and OD78, respectively. The A_{1g} SC decaying component in OD samples is negative (for OD78 in Fig. 3(c) and for OD52 and OD66 in SM Fig. S7), while those in UD74 and OP90 are positive. The sign change close to the optimal doping is also in good agreement with that of OPOP measurements in Bi2212 [31], but contrasts with the A_{1g} THz Kerr component which remains positive for all the samples studied. In addition, it is also apparent that the amplitudes of the A_{1g} and B_{1g} THz Kerr components in the SC state strongly depend on doping. Since $\Delta R/R$ depends on $\partial R/\partial \varepsilon_1$ at 800 nm, which in turn depends on doping, the evolution of the symmetry component of $\chi^{(3)}$ with doping can be best tracked in terms of the ratio of the B_{1g} and the A_{1g} THz Kerr components as summarized in Fig. 3(d) at 10 K. While the B_{1g} component is more than an order of magnitude weaker than the A_{1g} component in UD samples, it continuously increases with doping but never exceeds the A_{1g} component in the doping range studied, p = 0.10 - 0.22.

We now compare the experimental results with theoretical analysis, focusing on the origin of the symmetry-dependent THz Kerr signal observed in the SC state. As in the case of the THG, both CDF and Higgs mode can contribute to $\chi^{(3)}$. To quantify the magnitudes of these contributions in a symmetry-classified manner, we employ the single-band tight-binding model for Bi2212 to calculate $\chi^{(3)}$ numerically in the mean-field treatment (see SM). Let us first indicate, in Table 1, the general behavior of the symmetry decompositions

for the CDF and Higgs mode, respectively (see SM for details). While the CDF appears in all the symmetry channels, the Higgs mode selectively appears in the A_{1g} symmetry alone. If we then look at the numerical result for CDF, displayed in Fig. 4, we can see that all the contributions grow below T_c, and hence are correlated with superconductivity. Within the CDF, the B_{1g} channel exhibits by far the largest contribution. This is because $\chi^{(3)}_{xxxx}$ and $\chi^{(3)}_{xxyy}$ terms have opposite signs due to the band structure of the cuprates near the Fermi surface (see SM). Since $\chi^{(3)}_{A_{1g}} = \chi^{(3)}_{xxxx} + \chi^{(3)}_{xxyy}$ and $\chi^{(3)}_{B_{1g}} = \chi^{(3)}_{xxxx} - \chi^{(3)}_{xxyy}$, the two terms tend to cancel with each other in the A_{1g} symmetry, while they do not in B_{1g}. The B_{2g} component, being proportional to the square of the subdominant second-neighbor hopping, becomes smaller than the other symmetry components. Although the respective weights of the Higgs-mode and CDF contributions can depend on the level of approximations used in theoretical treatments [20], we expect the symmetry dependence of the CDF contribution to be robust because it is essentially tied to the band structure as elucidated above.

As we have seen, the A_{1g} THz Kerr component is experimentally dominant in all the samples studied. This strongly implies that the A_{1g} THz Kerr component originates from the Higgs-mode contribution of the *d*-wave order parameter, while the B_{1g} THz Kerr component likely originates from CDF. The absence of the B_{2g} CDF component in our measurement agrees with the mean-field result, in which it is about 17 times smaller than the B_{1g} contribution. The above interpretation is also supported by a comparison with Raman results in Bi2212, which are commonly attributed to CDF [43]. First, the increase in the relative amplitude of the B_{1g} component with doping is consistent with the strong increase in the pair-breaking peak intensity observed in B_{1g} Raman spectra toward $p = 0.22$ [38,44]. Second, in underdoped Bi2212 samples both B_{1g} and A_{1g} SC Raman responses vanish, leaving only a weak B_{2g} Raman signature of the SC state [45,46]. It was interpreted as a consequence of the PG opening which strongly suppresses the CDF response coming from anti-nodal QPs, but leaves intact the nodal QP probed in B_{2g} response [46]. This contrasts strongly with the dominance of the A_{1g} component observed here in UD samples in the THz Kerr signal, which further reinforces our assignment as arising from the *d*-wave Higgs mode.

Precise physical origin of the dominance of the Higgs-mode contribution to the THz Kerr effect remains an open problem. This may be a general property of nonlinear susceptibilities in the SC state at THz frequencies, since the same observation was deduced

from the polarization dependence of the THz THG signal in the conventional *s*-wave NbN [20]. A recent dynamical mean-field theory (DMFT) calculation has shown, as mentioned above, that the Higgs-mode contribution can actually exceed the CDF contribution if retardation effects are considered in strongly electron-phonon-coupled superconductors [20]. An interesting future problem then is whether this also holds for unconventional superconductors.

In conclusion, we have studied THz pulse-induced nonequilibrium dynamics in Bi2212 from the change in the optical reflectivity. We observed an oscillatory behavior of the optical reflectivity proportional to $|E_{\mathrm{Pump}}(t)|^2$ which we assign to a nonlinear THz Kerr effect. The signal is strongly enhanced below T_c, which we have decomposed into the A_{1g} and B_{1g} components. A theoretical calculation of the relevant third-order nonlinear susceptibility indicates that the A_{1g} component corresponds to the Higgs mode, while the B_{1g} component originates from CDF.

We acknowledge Dirk Manske for fruitful discussions. This work was partially supported by JSPS KAKENHI Grant Nos. 15H02102, 16K17729, JP26247057, and JP25800175 and by the Photon Frontier Network Program from MEXT, Japan. H.A. is also supported by ImPACT Program of Council for Science, Technology and Innovation, Cabinet Office, Government of Japan (Grant No. 2015-PM12-05-01) from JST. Y.G. acknowledges financial support for the Japan Society for the Promotion of Science (JSPS). Work at Brookhaven was supported by the Office of Basic Energy Sciences (BES), Division of Materials Sciences and Engineering, U.S. Department of Energy (DOE), through Contract No. de-sc0012704. RDZ and JS were supported by the Center for Emergent Superconductivity, an Energy Frontier Research Center funded by BES.

Figure captions

Figure 1 (Color online) (a) A geometry for the THz pump-optical probe measurements. (b) A schematic CuO_2 plane, on which the pump (θ_{Pump}) and probe (θ_{Probe}) polarization angles are defined relative to the Cu-O bond. (c) THz pulse-induced transient reflectivity change $\Delta R/R$ at $\theta_{Probe} = 0°$ as a function of delay time at typical temperatures for OP90. Top panel shows the waveform of the squared THz E-field. (d) Probe polarization dependence (circles) of the amplitude of $\Delta R/R$ at fixed delays at various temperatures for OP90 when $\theta_{Pump} = 0°$. Curves show the fitting with a form $A + B\cos(2\theta_{Probe})$.

Figure 2 (Color online) For OP90, temperature dependences of the A_{1g} (a) and B_{1g} (b) components of $\Delta R/R$ are displayed with red dashed lines indicating T_c. (c) The A_{1g} and B_{1g} components against the delay time at 10 K with fitting curves. (d) Temperature dependences of the A_{1g} decaying component (blue), the A_{1g} THz Kerr component (red), and the B_{1g} THz Kerr component (green).

Figure 3 (Color online) (a)-(c) Temporal behavior of the A_{1g} and B_{1g} components as compared for UD74, OP90, and OD78 at 10 K. Red and blue curves represent the A_{1g} THz Kerr component and decaying component, respectively, while black lines are total fitting curves. (d) Doping dependence of the ratio of the amplitude of the B_{1g} and the A_{1g} THz Kerr components at 10 K (red circles; left axis) with T_c (blue; right axis) for all the samples studied. The hole concentration p is determined from T_c with Presland and Tallon's equation [47].

Figure 4 (Color online) Numerical result for the CDF contribution to $\chi^{(3)}(\omega; \omega, +\Omega, -\Omega)$ for various symmetry components.

Table 1 General polarization dependence of CDF and Higgs-mode contributions for the TPOP measurements.

References

[1] D. Pekker and C. M. Varma, Annu. Rev. Condens. Matter Phys. **6**, 269 (2015).

[2] R. Matsunaga and R. Shimano, Phys. Scr **92**, 24003 (2017).

[3] R. Sooryakumar and M. V. Klein, Phys. Rev. Lett. **45**, 660 (1980).

[4] P. B. Littlewood and C. M. Varma, Phys. Rev. Lett. **47**, 811 (1981).

[5] M. A. Méasson, Y. Gallais, M. Cazayous, B. Clair, P. Rodière, L. Cario, and A. Sacuto, Phys. Rev. B **89**, 060503(R) (2014).

[6] R. Matsunaga, Y. I. Hamada, K. Makise, Y. Uzawa, H. Terai, Z. Wang, and R. Shimano, Phys. Rev. Lett. **111**, 057002 (2013).

[7] A. F. Volkov and S. M. Kogan, Zh. Eksp. Teor. Fiz **65**, 2038 (1973); [Sov. Phys. JETP 38, 1018 (1974)].

[8] Y. Barlas and C. M. Varma, Phys. Rev. B **87**, 054503 (2013).

[9] F. Peronaci, M. Schiró, and M. Capone, Phys. Rev. Lett. **115**, 257001 (2015).

[10] H. Krull, N. Bittner, G. S. Uhrig, D. Manske, and A. P. Schnyder, Nat. Commun. **7**, 11921 (2016).

[11] Y. Murotani, N. Tsuji, and H. Aoki, Phys. Rev. B **95**, 104503 (2017).

[12] B. Nosarzewski, B. Moritz, J. K. Freericks, A. F. Kemper, and T. P. Devereaux, arXiv:1609.04080v1 (2016).

[13] W. Fu, L.-Y. Y. Hung, and S. Sachdev, Phys. Rev. B **90**, 024506 (2014).

[14] A. Moor, P. A. Volkov, A. F. Volkov, and K. B. Efetov, Phys. Rev. B **90**, 024511 (2014).

[15] Z. M. Raines, V. G. Stanev, and V. M. Galitski, Phys. Rev. B **92**, 184511 (2015).

[16] R. Soto-Garrido, Y. Wang, E. Fradkin, and S. L. Cooper, Phys. Rev. B **95**, 214502 (2017).

[17] R. Matsunaga, N. Tsuji, H. Fujita, A. Sugioka, K. Makise, Y. Uzawa, H. Terai, Z. Wang, H. Aoki, and R. Shimano, Science **345**, 1145 (2014).

[18] N. Tsuji and H. Aoki, Phys. Rev. B **92**, 064508 (2015).

[19] T. Cea, C. Castellani, and L. Benfatto, Phys. Rev. B **93**, 180507(R) (2016).

[20] R. Matsunaga, N. Tsuji, K. Makise, H. Terai, H. Aoki, and R. Shimano, Phys. Rev. B **96**, 020505(R) (2017).

[21] N. Tsuji, Y. Murakami, and H. Aoki, Phys. Rev. B **94**, 224519 (2016).

[22] See Supplemental Material for details of the experimental setup, data analysis and theoretical calculations, which includes Refs. [23–27].
[23] J. Hebling, G. Almasi, I. Kozma, and J. Kuhl, Opt. Express **10**, 1161 (2002).
[24] S. Watanabe, N. Minami, and R. Shimano, Opt. Express **19**, 1528 (2011).
[25] A. Rothwarf and B. N. Taylor, Phys. Rev. Lett. **19**, 27 (1967).
[26] P. W. Anderson, Phys. Rev. **112**, 1900 (1958).
[27] A. A. Kordyuk, S. V. Borisenko, M. Knupfer, and J. Fink, Phys. Rev. B **67**, 064504 (2003).
[28] J. Demsar, B. Podobnik, V. V. Kabanov, T. Wolf, and D. Mihailovic, Phys. Rev. Lett. **82**, 4918 (1999).
[29] V. V Kabanov, J. Demsar, B. Podobnik, and D. Mihailovic, Phys. Rev. B **59**, 1497 (1999).
[30] V. V. Kabanov, J. Demsar, and D. Mihailovic, Phys. Rev. Lett. **95**, 147002 (2005).
[31] N. Gedik, M. Langner, J. Orenstein, S. Ono, Y. Abe, and Y. Ando, Phys. Rev. Lett. **95**, 117005 (2005).
[32] Y. H. Liu, Y. Toda, K. Shimatake, N. Momono, M. Oda, and M. Ido, Phys. Rev. Lett. **101**, 137003 (2008).
[33] Y. Toda, T. Mertelj, P. Kusar, T. Kurosawa, M. Oda, M. Ido, and D. Mihailovic, Phys. Rev. B **84**, 174516 (2011).
[34] G. Coslovich, C. Giannetti, F. Cilento, S. Dal Conte, G. Ferrini, P. Galinetto, M. Greven, H. Eisaki, M. Raichle, R. Liang, A. Damascelli, and F. Parmigiani, Phys. Rev. B **83**, 064519 (2011).
[35] B. Mansart, J. Lorenzana, A. Mann, A. Odeh, M. Scarongella, M. Chergui, and F. Carbone, Proc. Natl. Acad. Sci. **110**, 4539 (2013).
[36] Y. Toda, F. Kawanokami, T. Kurosawa, M. Oda, I. Madan, T. Mertelj, V. V. Kabanov, and D. Mihailovic, Phys. Rev. B **90**, 094513 (2014).
[37] H. Anzai, A. Ino, M. Arita, H. Namatame, M. Taniguchi, M. Ishikado, K. Fujita, S. Ishida, and S. Uchida, Nat. Commun. **4**, 1815 (2013).
[38] S. Benhabib, A. Sacuto, M. Civelli, I. Paul, M. Cazayous, Y. Gallais, M. A. Méasson, R. D. Zhong, J. Schneeloch, G. D. Gu, D. Colson, and A. Forget, Phys. Rev. Lett. **114**, 147001 (2015).
[39] M. C. Hoffmann, N. C. Brandt, H. Y. Hwang, K. Lo Yeh, and K. A. Nelson, Appl. Phys. Lett. **95**, 231105 (2009).
[40] R. W. Boyd, *Nonlinear Optics*, 3rd ed (Academic Press, 2008).
[41] H. Yada, T. Miyamoto, and H. Okamoto, Appl. Phys. Lett. **102**, 091104 (2013).

[42] M. Hashimoto, I. M. Vishik, R.-H. He, T. P. Devereaux, and Z.-X. Shen, Nat. Phys. **10**, 483 (2014).

[43] T. P. Devereaux and R. Hackl, Rev. Mod. Phys. **79**, 175 (2007).

[44] M. Opel, R. Nemetschek, C. Hoffmann, R. Philipp, P. F. Müller, R. Hackl, I. Tüttő, A. Erb, B. Revaz, E. Walker, H. Berger, and L. Forró, Phys. Rev. B **61**, 9752 (2000).

[45] S. Sugai and T. Hosokawa, Phys. Rev. Lett. **85**, 1112 (2000).

[46] S. Blanc, Y. Gallais, M. Cazayous, M. A. Méasson, A. Sacuto, A. Georges, J. S. Wen, Z. J. Xu, G. D. Gu, and D. Colson, Phys. Rev. B **82**, 144516 (2010).

[47] M. R. Presland, J. L. Tallon, R. G. Buckley, R. S. Liu, and N. E. Flower, Phys. C **176**, 95 (1991).

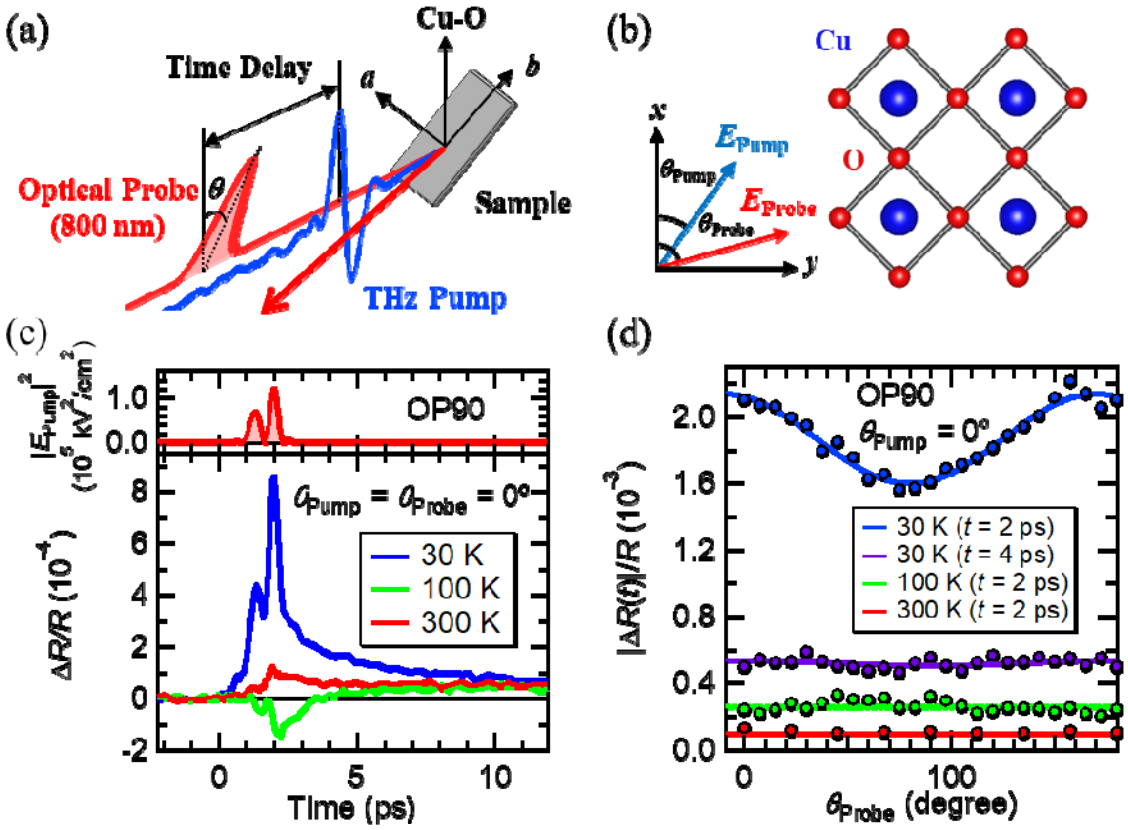

Figure 1

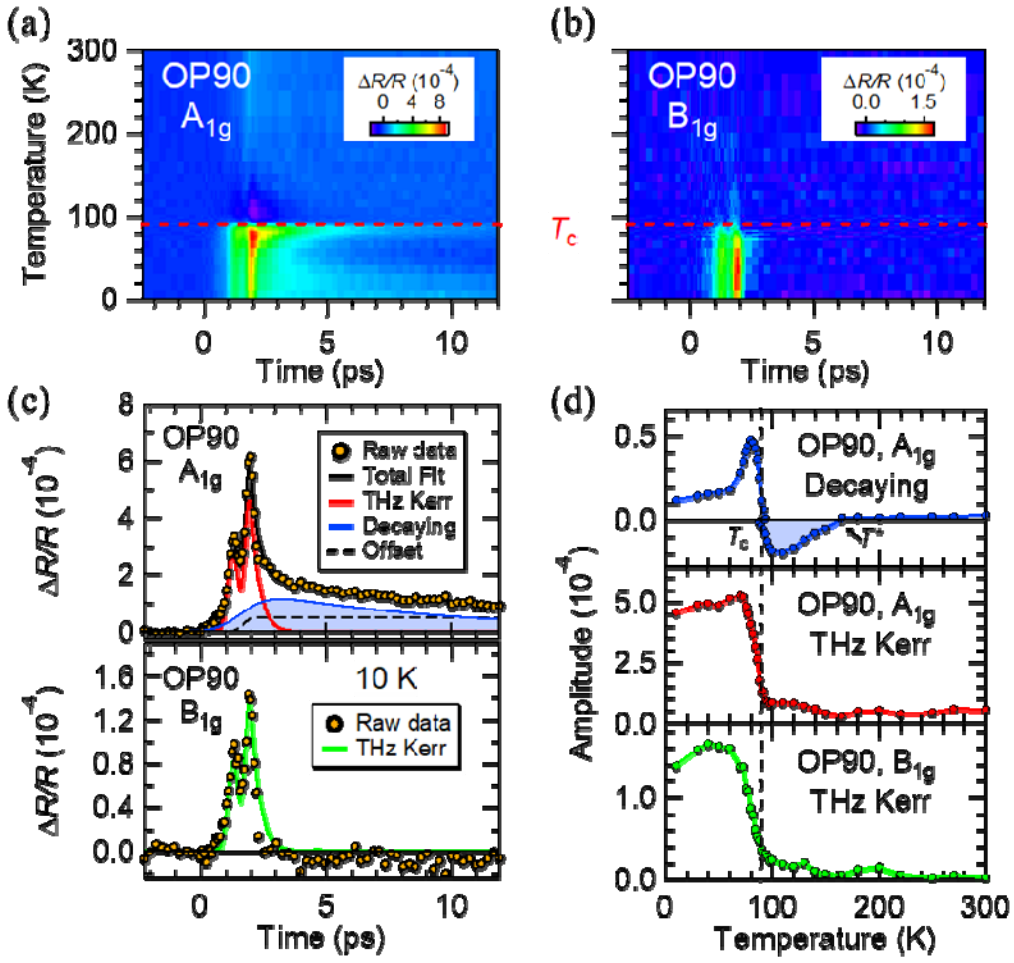
(a)
OP90
A1g
ΔR/R (10-4)
0 4 8
Temperature (K)
300
200
100
0
0 5 10
Time (ps)
(b)
OP90
B1g
ΔR/R (10-4)
0.0 1.5
Tc
0 5 10
Time (ps)
(c)
OP90
A1g
Raw data
Total Fit
THz Kerr
Decaying
Offset
ΔR/R (10-4)
8 6 4 2 0
OP90
B1g
10 K
Raw data
THz Kerr
ΔR/R (10-4)
1.6 1.2 0.8 0.4 0.0
0 5 10
Time (ps)
(d)
OP90, A1g
Decaying
Tc
Γ*
0.5 0.0
OP90, A1g
THz Kerr
5.0 2.5 0.0
OP90, B1g
THz Kerr
1.0 0.0
Amplitude (10-4)
0 100 200 300
Temperature (K)

Figure 2

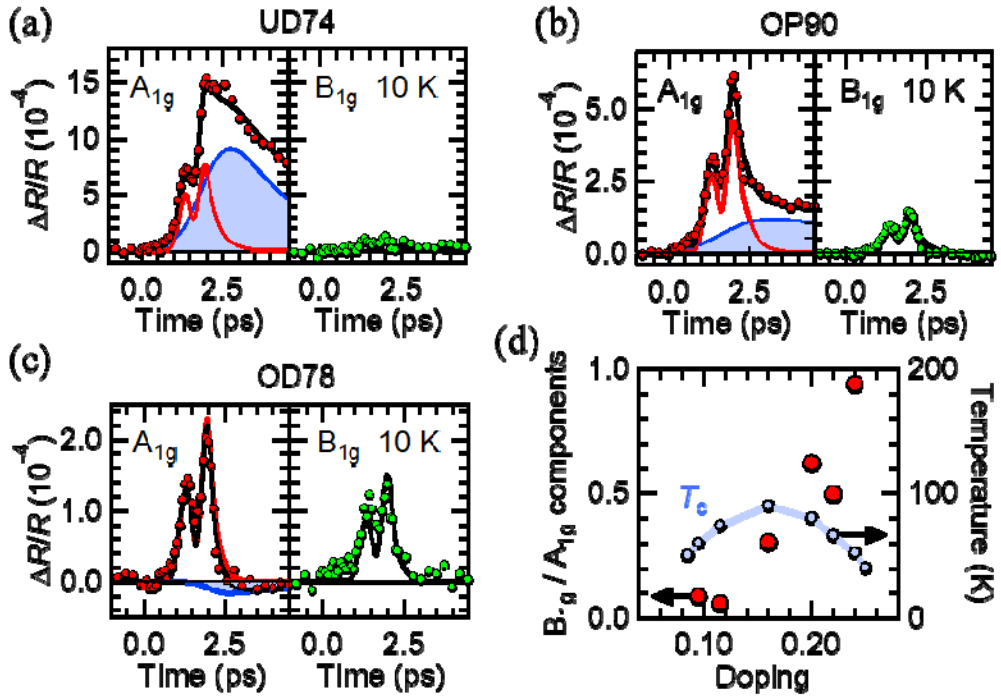

Figure 3

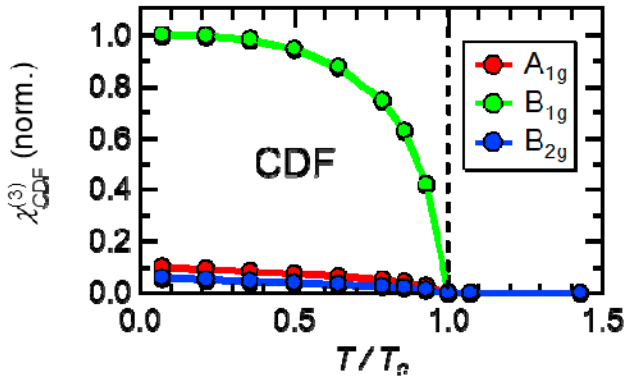

Figure 4

Table 1

	A_{1g}	B_{1g}	B_{2g}
CDF	□	□	□
Higgs	□	0	0